JCTC Journal of Chemical Theory and Computation

ARTICLE

pubs.acs.org/JCTC

First Principles-Based Calculations of Free Energy of Binding: Application to Ligand Binding in a Self-Assembling Superstructure

Stephen Fox,[†] Hannes G. Wallnoefer,[‡] Thomas Fox,[‡] Christofer S. Tautermann,[‡] and Chris-Kriton Skylaris*[,†]

[†]School of Chemistry, University of Southampton, Southampton, Hampshire SO17 1BJ, United Kingdom

[‡]Department for Lead Identification and Optimization Support, Boehringer Ingelheim Pharma GmbH & Co KG, 88397 Biberach, Germany

ABSTRACT: The accurate prediction of ligand binding affinities to a protein remains a desirable goal of computational biochemistry. Many available methods use molecular mechanics (MM) to describe the system, however, MM force fields cannot fully describe the complex interactions involved in binding, specifically electron transfer and polarization. First principles approaches can fully account for these interactions, and with the development of linear-scaling first principles programs, it is now viable to apply first principles calculations to systems containing tens of thousands of atoms. In this paper, a quantum mechanical Poisson−Boltzmann surface area approach is applied to a model of a protein−ligand binding cavity, the "tennis ball" dimer. Results obtained from this approach demonstrate considerable improvement over conventional molecular mechanics Poisson−Boltzmann surface area due to the more accurate description of the interactions in the system. For the first principles calculations in this study, the linear-scaling density functional theory program ONETEP is used, allowing the approach to be applied to receptor−ligand complexes of pharmaceutical interest that typically include thousands of atoms.

1. INTRODUCTION

With the growing number of experimentally determined 3D molecular structures refined to a high atomic resolution, molecular modeling is expanding its role in understanding structure/function relationships of biomolecules. Techniques of increasing sophistication are available for describing atomic forces, ranging from classical molecular mechanics (MM) with coarse grained or atomistic force fields to first principles electronic structure calculations.[1] Computational simulations with these techniques can be used to calculate structural, dynamic, and thermodynamic properties and have found wide usage as tools for assessing potential pharmaceutical drugs and for potentially reducing the need for experimental work.

A central problem in drug discovery is the prediction of receptor−ligand binding free energies. Among the many approaches available for free energy calculations, docking and scoring[2] are among the least computationally expensive but also most approximate. In these methods ligand orientations (poses) are assigned scores, and the quality of the fit is expressed by an empirical function, the scoring function. These scores are used to rank each pose relative to other poses and other ligands. Methods with a higher level of statistical mechanics rigor include molecular mechanics Poisson−Boltzmann surface area (MM-PBSA)[3] and molecular mechanics generalized Born surface area (MM-GBSA).[4] These methods estimate absolute free energies of bound and unbound reference states using molecular dynamics (MD) simulations to sample phase space. Free energies of binding are obtained as averages of interaction energies over snapshots from the MD simulations with entropic contributions calculated from vibrational frequency calculations and the solvation free energy contributions from an implicit solvent model. Although this approach has found extensive usage, especially for the calculation of relative free energies of binding, its accuracy is limited by the approximate nature of including entropy and solvation effects as well as the force field, which is required to reproduce structures and energies with high accuracy. At the most theoretically rigorous end of the spectrum we have methods, such as potentials of mean force and alchemical free energy calculation approaches.[5] An example of an alchemical method is thermodynamic integration (TI). It follows an unphysical pathway, where one ligand is mutated to another. It evaluates ratios of partition functions to estimate relative binding free energies and their gradual change during the mutation, which happens in small steps and fully includes the entropic and solvation contributions which are heavily approximated with the less rigorous approaches. In principle, alchemical free energy calculations allow the exact prediction of relative binding free energies, at very high computational cost. However, inadequacies in the force fields used and insufficient sampling introduce errors into the calculated free energies. These errors are exacerbated by ligands that cause changes which are difficult to capture by classical force fields, such as charge transfer and polarization or conformational change on binding, which may require extremely long simulations.

A large number of force fields have been developed and extensively parametrized for common amino acids found in proteins, but the development and parametrization of force fields for general ligands are a much more difficult task. Even in the protein force fields there are issues with their transferability and accuracy, as their form can allow only for an average picture of electronic polarization and no inclusion of electronic charge transfer; yet these effects are ubiquitous and can often make important contributions to energies and structures. Promising progress is being made into polarizable force fields,[6] but these approaches

Received: December 9, 2010
Published: March 16, 2011

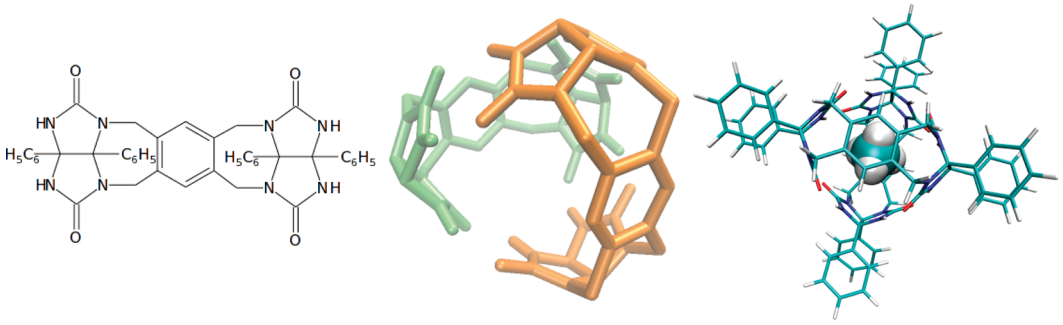

Figure 1. Two-dimensional (2D) diagram of the monomer (left). Truncated structure of the tennis ball depicting the shape of the cavity (middle). Encapsulation of a methane molecule in the whole dimer (right).

are still not as general or as able to achieve the required levels of accuracy.

First principles quantum mechanical (QM) methods explicitly include the electrons and therefore can fully take into account the electronic charge transfer and polarization and are transferable to any chemical environment. They are therefore ideal for biomolecular simulations, since the interactions between ligand and receptor always involve rearrangement of electrons to a certain extent, and first principles calculations would be expected to provide more accurate binding free energies. The most widely used first principles approach is Kohn−Sham density functional theory (DFT),[7] as it offers a good compromise between accuracy and computational cost. However, the applicability of first principles calculations in such simulations is limited because in general they are 1000 times more computationally demanding than force field approaches, and more importantly, their computational cost increases with the third power in the number of atoms. In practice this limits the size of the calculations to a few hundred atoms at most, while most biomolecular systems of interest tend to include thousands of atoms. In cases where quantum calculations are unavoidable, such as for example, in the study of chemical reactions in the active sites of enzymes, small parts of the active site are simulated using quantum mechanics while the rest of the system is described by a classical force field. A variety of such QM/MM approaches have been developed,[8,9] but their application requires extensive experience in order to effect a physically meaningful partition of the system to QM and MM regions and also to properly describe the interaction between these two fundamentally different models. An alternative approach would be to perform first principles calculations on the entire biomolecular system if there was a way to avoid their cubic scaling cost. This can be achieved by using linear-scaling first principles approaches[10] which have the capability for calculations on many thousands of atoms. The development of such approaches has been slow, as it required dealing with a variety of nontrivial physical and computational issues, but today a number of linear-scaling DFT packages are available such as ONETEP,[11] CONQUEST,[12] SIESTA,[13] and others.[14]

In this work we are evaluating the use of first principles calculations in combination with a classical force field to simulate host−guest interactions. The system we have selected to study is a model for a protein ligand-binding cavity based on a self-assembling superstructure, the "tennis ball" dimer (Figure 1). We have chosen this model as it combines simplicity with realism and also because there are previous computational[15] studies and experimental[16] data to compare with. We first compare structure optimization with a force field and first principles approaches in terms of the structural parameters. We then introduce dynamic effects through MD simulations and compare binding energies calculated from MM-PBSA and QM-PBSA to experimental values. For our first principles calculations we use linear-scaling DFT as implemented in the ONETEP[11] program which has a demonstrated capability for DFT calculations with thousands of atoms.[17] These are the length scales of several proteins of relevance to current therapeutical challenges, and therefore the use of linear-scaling DFT will allow, with further future testing and validation, the application of first principles-based simulations to some of these proteins.

In Section 2.1 the ONETEP approach is discussed. Section 2.2 will detail the computational methods used in this study. Section 2.3 will outline the procedure and parameters. In Section 3 the results are given and analyzed, and Section 4 summarizes our results and conclusions.

2. METHODS

2.1. The ONETEP Approach. The ONETEP[11] program is a linear-scaling DFT code that has been developed for use on parallel computers.[18] ONETEP combines linear scaling with accuracy comparable to conventional cubic-scaling plane-wave methods, which provide an unbiased and systematically improvable approach to DFT calculations. Its novel and highly efficient algorithms allow calculations on systems containing tens of thousands of atoms.[17] ONETEP is based on a reformulation of DFT in terms of the one-particle density matrix. The density matrix in terms of Kohn−Sham orbitals is

$$\rho(\mathbf{r},\mathbf{r}') = \sum_{n=0}^{\infty} f_n \psi_n(\mathbf{r}) \psi_n^*(\mathbf{r}') \qquad (1)$$

where f_n is the occupancy and $\psi_n(\mathbf{r})$ and $\psi_n(\mathbf{r}')$ are the Kohn−Sham orbitals. In ONETEP the density matrix is represented as

$$\rho(\mathbf{r},\mathbf{r}') = \sum_{\alpha}\sum_{\beta} \phi_\alpha(\mathbf{r}) K^{\alpha\beta} \phi_\beta^*(\mathbf{r}') \qquad (2)$$

where $\phi_\alpha(\mathbf{r})$ is the localized nonorthogonal generalized Wannier functions[19] (NGWFs) and $K^{\alpha\beta}$, which is called the density kernel, is the representation of f_n in the duals of these functions. Linear-scaling is achieved by truncation of the density matrix, which decays exponentially for materials with a band gap and by enforcing strict localization of the NGWFs onto atomic regions. In ONETEP as well as optimizing the density kernel, the NGWFs are also optimized, subject to a localization

constraint. Optimizing the NGWFs in situ allows for a minimum number of NGWFs to be used while still achieving plane-wave accuracy. The NGWFs are expanded in a basis set of periodic sinc (psinc) functions,[20] which are equivalent to a plane-wave basis as they are related by a unitary transformation. Using a plane-wave basis set allows the accuracy to be improved by changing a single parameter, equivalent to the energy cutoff in conventional plane-wave DFT codes. The psinc basis set provides a uniform description of space, meaning that ONETEP does not suffer from basis set superposition error.[21]

2.2. MM-PBSA and QM-PBSA. The MM-PBSA[3] approach is commonly used to calculate relative (and absolute) binding affinities of small molecules to proteins via differences between bound and unbound states. Representative structural ensembles are generated by MD simulations in explicit solvent. Snapshots are extracted at constant time intervals, and the solvent molecules and counterions are removed. Binding energy calculations are then performed on the individual structures using the MM force field together with an implicit solvent approach (PBSA). The free energy of binding is then obtained as an average over the ensemble binding energies. In the solvent model the polar solvent contributions are calculated via the Poisson−Boltzmann (PB) equation, and the nonpolar solvent contributions are calculated from the solvent accessible surface area (SA). The free energy of binding is calculated according to

$$\Delta G_{\text{bind}} = \langle \Delta H_{\text{vac}} \rangle + \langle \Delta G_{\text{solv}} \rangle - T\langle \Delta S \rangle$$
$$= \langle \Delta H_{\text{vac}} \rangle + \langle \Delta G_{\text{solv}}^{\text{polar}} \rangle + \langle \Delta G_{\text{solv}}^{\text{nonpolar}} \rangle - T\langle \Delta S \rangle \quad (3)$$

Where $\langle \Delta H_{\text{vac}} \rangle$ arises from the average difference in van der Waals and electrostatic contributions from the MM force field, $\langle \Delta G_{\text{solv}} \rangle$ is the average free energy of solvation from the PBSA model, and $\langle \Delta S \rangle$ is the entropy of binding which is approximated from harmonic vibrational frequency calculations averaged over the snapshots. A common assumption is that similar ligands bound to the same receptor contribute comparably to the binding entropy, and hence this term is often omitted from the calculations. The difference in free energies of binding between two ligands, A and B, is then given by

$$\Delta\Delta G_{\text{A}\rightarrow\text{B}} = \Delta\langle \Delta H_{\text{vac}} \rangle_{\text{A}\rightarrow\text{B}} + \Delta\langle \Delta G_{\text{solv}} \rangle_{\text{A}\rightarrow\text{B}} \quad (4)$$

The MM-PBSA method used in this study is the single-trajectory approach. In this approach the receptor and ligand structures are taken from the geometry of the complex. It has been observed that this approach produces relative free energies of binding that converge faster with the number of snapshots sampled and are also more accurate, compared to the three-trajectory approach, due to cancellation of errors.[22]

A significant source of error in MM-PBSA can be the accuracy of the interaction energies computed for each snapshot, as this depends on the selected force field. Several attempts have been made toward overcoming these limitations by the inclusion of the rigor of quantum mechanics in QM-PBSA extensions of the MM-PBSA approach, which uses semiempirical QM[23] or hybrid QM/MM.[24,25]

More recently a QM-PBSA approach[26] has been presented, where the calculation of the interaction energies by the force field is replaced by DFT calculations on the entire molecules involved. In more detail, the energy of each snapshot is obtained as $E_{\text{QM}} = E_{\text{DFT}} + E_{\text{disp}}$, where E_{disp} is the dispersion correction[27] to the total DFT energy, E_{DFT}. The free energy of solvation for each snapshot from the MM-PBSA calculation is scaled to match the electrostatics of the QM calculation in the following way:

$$\Delta G_{\text{solv}}^{\text{QM}} = \Delta G_{\text{solv}}^{\text{MM}} \left(\frac{\Delta E_{\text{QM}}}{\Delta E_{\text{MM}}} \right) \quad (5)$$

where ΔE_{MM} is the total binding energy from the MM force field, and, as in usual MM-PBSA, is averaged over the snapshots and added to the total DFT energy to give the free energy of binding as

$$\Delta G_{\text{tot}} = \langle \Delta E_{\text{QM}} \rangle + \langle \Delta G_{\text{solv}}^{\text{QM}} \rangle \quad (6)$$

The scaling method used in previous works[26] scaled the solvation energy by the fraction of the electrostatic components of the binding energy. In our system that scaling method does not work since dispersion interactions are responsible for most of the binding energy, leading to the MM electrostatic component of the binding energy in the denominator, being very close to zero. We found that the simpler form shown in eq 5 produces reasonable solvation energies.

The first application of QM-PBSA[26] has been on protein−protein interactions. The results obtained were in good agreement with the MM-PBSA, most likely because the force field employed has been extensively and carefully parametrized for protein systems and improved over a number of years. As our present system does not consist of amino acids, we do not have the advantage of using such a well-developed force field. This is a situation which is common in drug design as nonstandard residues and new ligands are explored and the reliability of a general force field needs to be checked on a case by case basis. Here we are aiming to investigate how QM-PBSA can be used in such a case, as a an accuracy benchmark for MM-PBSA or as an alternative approach.

2.3. Simulation Details. The tennis ball structure was built and loosely minimized with the MOE[28] program. MM simulations were carried out using the AMBER 10[29] package. The tennis ball was modeled using the generalized AMBER force field[30] (gaff) and solvated with the $CHCl_3$ explicit solvent model (as implemented in AMBER 10) in a periodic box.

To equilibrate the system, the hydrogens were relaxed keeping all heavy atoms restrained in the host and solvent, then relaxing the solvent with restraints still on the host. The system was heated to 300 K still restraining the host for 200 ps with the NVT ensemble and ran for a further 200 ps with the NPT ensemble at 300 K in order to equilibrate the solvent density. This was cooled to 100 K over 100 ps and minimization's carried out reducing the restraints on the host heavy atoms in stages (500, 100 ,50, 20, 10, 5, 2, 1, and 0.5 kcal mol^{-1} Å^{-2}). Finally the system was heated to 300 K with no restraints over 200 ps and then ran for a further 200 ps at 300 K with the NPT ensemble, at the end of which the root mean squared deviation of the carbon, nitrogen, and oxygen atoms was converged and less than 0.8 Å relative to the starting frame. production simulations were run for 2 ns with the NPT ensemble at 300 K. All MD simulations used the Langevin thermostat, the particle mesh Ewald (PME) sum for the electrostatic interactions, a time-step of 2 fs, and the SHAKE algorithm.[31] For the MM-PBSA calculation an infinite nonbonded cutoff was used with a dielectric constant of 4.5 to represent the chloroform solvent. All ONETEP single-point energies were converged to 0.0002 hartree (∼0.1 kcal mol^{-1}). Four NGWFs were used to describe carbon, oxygen and

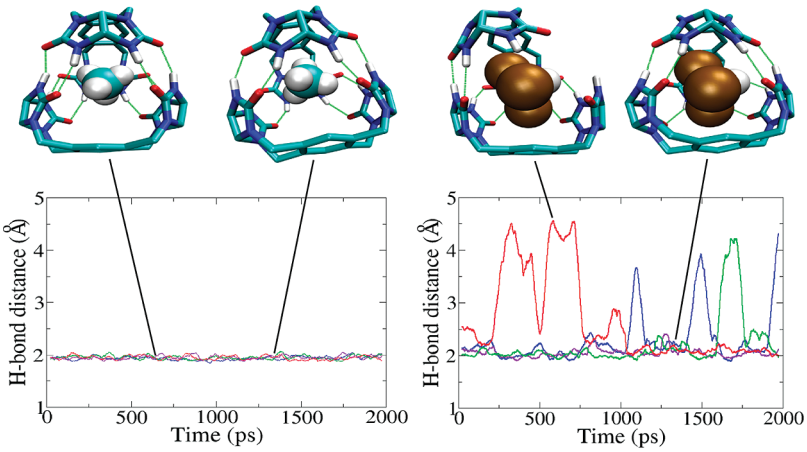

Figure 2. Plots of the hydrogen-bond lengths from four hydrogen-bonding positions (C═O′s of top monomer to H—N′s of bottom monomer) in the CH_4 complex (left) and $CHCl_3$ complex (right). Structures taken as "snapshots" at two points of the simulations are shown, the green dashed lines represent the hydrogen bonds present at each snapshot. In the graphs, the four colored lines correspond to the four hydrogen bonds measured in each complex (phenyl rings not displayed).

nitrogen, 1 for hydrogens and 9 NGWFs for the halogen atoms. A kinetic energy cutoff of 800 eV for the psinc basis set was used, with the GGA exchange−correlation functional PBE[32] combined with our implementation of the DFT+D approach to account for dispersion parametrized specifically for this functional.[27]

3. RESULTS AND DISCUSSION

3.1. Validation tests. In cases where two different approaches are used to explore the conformational space, the compatibility of the methods used is an important consideration.[33] First, it is desirable that the minima on the potential energy surface between the QM and the MM approach are as close as possible. To investigate this we have carried out geometry optimizations of the three complexes using ONETEP and AMBER. We have also carried out further validation of the QM approach by doing the same geometry optimizations with the Gaussian[34] program which can perform all-electron DFT calculations with Gaussian basis sets. For these all-electron calculations we used a correlation consistent split valence basis set (cc-pVDZ[35]) and the B97 exchange−correlation functional[36] with the DFT+D approach for including dispersion contributions, as parametrized by Grimme et al.[37] The structural parameters between the optimized geometries by the three methods were compared. Bond lengths vary by less than 0.03 Å, and internal angles, such as those within rings, vary by less than 0.5, with the more flexible angles differing by 2−3. Hydrogen bonds from ONETEP (Gaussian) are shorter than these from the AMBER optimized structure by 0.2 Å (0.1 Å), and the distance separating the monomers differs by as much as 0.5 Å between the ONETEP and AMBER structures. All the methods predict hydrogen bonds which are longer by around 0.2 Å for the $CHCl_3$ complex compared to the tennis ball complexed with CH_4 or CF_4 and the empty dimer, which is to be expected as the $CHCl_3$ is slightly larger than the size of the empty cavity.

As we are interested in properties at finite temperatures (usually room temperature), using only equilibrium geometries is not sufficient, as dynamical motion causes the molecules to visit many configurations which can differ from the relaxed structures. Thus, MD simulations are run for time scales which are long enough (ns) to sample the dynamical behavior of this system, using the classical force field approach. The importance of accounting for dynamic motion for the tennis ball system is shown in Figure 2. Here we examine hydrogen-bond lengths in the CH_4 and $CHCl_3$ complexes throughout the 2 ns MD simulations. During the simulation, the hydrogen bonds in the CH_4 complex are stable, staying at around 2 Å. In contrast, the hydrogen bonds in the $CHCl_3$ complex are intermittent. We observe that the dimer opens at a point, around 4 Å, then moves back into position, re-establishes the hydrogen bond, and breaks at another point. This happens due to the size of the chloroform ligand; it is too large to fit comfortably between the monomers causing the cavity to open and close during the simulation. Figure 2 demonstrates that the $CHCl_3$ complex has one hydrogen-bond broken most of the time. In this case the minimum energy structure, which has all the hydrogen bonds intact, albeit elongated, will not provide an adequate description of the ensemble of structures encountered at room temperature. We can demonstrate this further by noting that the binding energy for the $CHCl_3$ complex as calculated with ONETEP on the optimized structure is 2.6 kcal mol^{-1}, while when taking into account 200 snapshots extracted from the MD ensemble, it is −7.1 kcal mol^{-1} (see Section 3.2), in close agreement with the experimental value of −7 kcal mol^{-1}. As a dynamical ensemble of structures is necessary for this study, we also need to confirm that the conformations sampled by the force field are not unphysical as far as the QM potential energy surface is concerned. To explore this issue, we have compared forces on atoms calculated from ONETEP and AMBER on several of the snapshots. An indication that the compatibility of the two approaches is good in this case is given by the values reported in Table 1, which presents the average (maximum) of the absolute values of the force on all

Table 1. Average (Maximum) of Forces on Atoms from AMBER and ONETEP from 10 Snapshots[a]

complex	ONETEP	AMBER
CH_4	29.3 (153.0)	29.9 (107.0)
$CHCl_3$	29.3 (147.8)	29.7 (105.0)
CF_4	30.1 (150.8)	30.1 (128.1)

[a] Values in kcal/mol/Å.

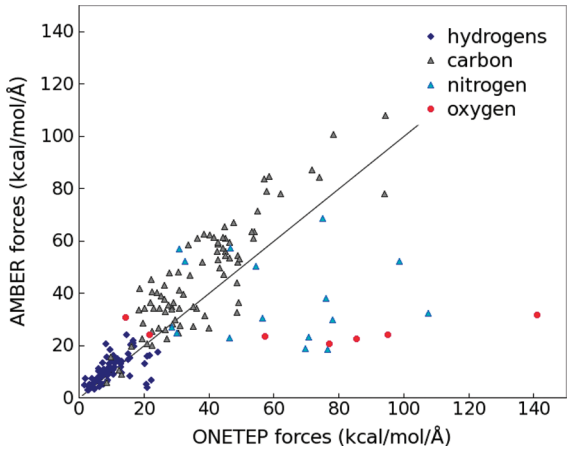

Figure 3. Correlation between $|F_{QM}|$ and $|F_{MM}|$ for a single snapshot of the CH_4 complex. Other snapshots and complexes show similar behavior.

Table 2. MM- and QM-PBSA Results Presenting Binding Free Energies Separated into Differences in Enthalpy and Free Energy and Relative Differences between Ligands Using CH_4 as a Reference[a]

	ΔH			ΔG		
	MM-PBSA	QM-PBSA	expt[16]	MM-PBSA	QM-PBSA	expt[16]
CH_4	-8.7 ± 0.05	-9.0 ± 0.04	-9	-8.5 ± 0.05	-8.9 ± 0.05	-3.0
$CHCl_3$	-16.8 ± 0.19	-7.1 ± 0.27	-7	-14.9 ± 0.16	-6.2 ± 0.23	2.2
CF_4	-12.6 ± 0.09	-6.0 ± 0.08	N/A	-11.9 ± 0.08	-5.7 ± 0.08	-0.2[15]

	$\Delta\Delta H$			$\Delta\Delta G$		
	MM-PBSA	QM-PBSA	expt[16]	MM-PBSA	QM-PBSA	expt[16]
$CH_4 \rightarrow CHCl_3$	-8.1	2.1	2	-6.4	2.7	5.2
$CH_4 \rightarrow CF_4$	-3.9	3.0	N/A	-3.4	3.2	2.8[15]

[a] ΔH is the energy in vacuum. ΔG is the vacuum energy plus the solvation energy (for MM- and QM-PBSA this term does not include conformational entropy).

atoms over 10 equally spaced snapshots. Even though these agree extremely well between the two approaches, if we look in more detail at individual atoms, the agreement is not so good. The largest difference between the QM and MM forces on any single atom is 80 kcal mol^{-1} $Å^{-1}$, but for most atoms, it is less than 20 kcal mol^{-1} $Å^{-1}$. Figure 3 compares the forces between QM and MM between individual atoms for a single snapshot of the CH_4 complex, colored according to the type of element. We can observe that for hydrogen and carbon atoms both ONETEP and AMBER forces agree reasonably well. The large differences on the oxygen and nitrogen atoms are as expected, this is because the parametrization of the ligand is done in group-wise fashion, so an amine-group will have a charge of one, but it is not clear how the charges are distributed over the atoms, thus the charges for heteroatoms will strongly differ from ONETEP causing a strong difference in gradient. This behavior is representative of all snapshots for the three systems. Our comparisons show that there is substantial variability in the forces obtained with the two approaches, however the forces in both cases are within expected ranges, and the average forces are comparable. This suggests that no unphysical conformations are visited by the force field.

Having established the importance of taking into account the dynamical behavior of this system, we finally tested the convergence of PBSA energies as a function of the number of MD snapshots. An increasing number of snapshots was used, obtained by sampling uniformly through the 2 ns production simulations. From each simulation, 50, 100, 160, and 200 equally spaced snapshots were extracted to study the convergence. We found that the variation in the binding free energies calculated in ONETEP or AMBER when going from 50 to 200 snapshots was less than 0.2 kcal/mol for all systems studied. All MM- and QM-PBSA results we report here were obtained using 200 snapshots.

Table 3. Relative Binding Free Energies (kcal/mol) Obtained via TI by Fox et al.[a]

	TI[15]	TI with gaff	QM-PBSA	MM-PBSA	expt[16]
$CH_4 \rightarrow CHCl_3$	7.8	7.2	2.8	-6.4	5.2
$CH_4 \rightarrow CF_4$	0.9	0.1	3.2	-3.4	2.8

[a] TI results using the gaff and results from our QM-PBSA approach.

3.2. Free Energies of Binding. The energies of binding that were obtained with the MM- and QM-PBSA approaches for all the complexes are presented in Table 2. The table shows the enthalpies of binding (ΔH) computed from either the force field or the DFT calculations with ONETEP and the free energy of binding (ΔG), which includes solvation contributions. We observe that for CH_4 AMBER predicts a ΔH that agrees well with experiment (to <0.3 kcal mol^{-1}), however it overestimates the ΔH for the halogen-containing ligands to over twice the experimental value. This suggests that the force field does not capture well the interaction energies of the halogen atoms with the cavity. ONETEP produces ΔH values that are in close agreement (within 0.1 kcal mol^{-1}) to the experimentally determined ΔH values, which supports further our earliest observation that the ensemble of structures provided by the force field has a high overlap with the QM ensemble. The larger standard errors in the calculated energy differences for the $CHCl_3$ complex, 0.27 kcal mol^{-1} compared to 0.04 kcal mol^{-1} for CH_4, are expected since this structure shows considerably more fluctuation than the other complexes, as we saw in Figure 2.

Since AMBER overestimates the interaction energies for the halogen-containing ligands, the calculated $\Delta\Delta G$'s predict a more favorable interaction than was found experimentally and in the previous computational study. Our improvements by the QM calculations refer to the enthalpic part of the binding energies, and indeed we can observe that the $\Delta\Delta H$ values are a very good match to experiment.

As the enthalpy is accounted for so well, and the free energy of solvation in this case makes a minimal contribution due to the nonaqueous solvent, the large discrepancy in the free energy differences ΔG can be attributed to the neglect of configurational entropy. When considering the $\Delta\Delta G$ values a large fraction of this error is canceled, and we obtain reasonably good agreement with experiment [2.7 versus 5.2 kcal mol^{-1} for $\Delta\Delta G(CH_4 \rightarrow CHCl_3)$ and 3.2 versus 2.8 kcal mol^{-1} for $\Delta\Delta G(CH_4 \rightarrow CF_4)$] for ONETEP, while the AMBER values show discrepancies of more than 5 kcal mol^{-1}, precisely due to the bad estimation of enthalpy.

Previous computational results by Fox et al.[15] were obtained from TI calculations. Simulations were performed with AMBER 4.1 using the all-atom force field by Cornell et al.[38] and the partial charges obtained from a multiple molecule RESP fit. Table 3 compares their results to TI free energies we obtained with AMBER 10 using the gaff force field and with our MM- and QM-

PBSA results. We observe that both TI approaches obtain comparable relative binding free energies (7.8 versus 7.2 kcal mol^{-1} for $CH_4 \rightarrow CHCl_3$ and 0.9 versus 0.1 kcal mol^{-1} for $CH_4 \rightarrow CF_4$) and considerably better than MM-PBSA ($\Delta\Delta G(CH_4 \rightarrow CHCl_3)$ of 7.8 kcal mol^{-1} rather than −6.4 kcal mol^{-1}). While TI is a more rigorous approach which fully accounts for entropic effects, we observe that our QM-PBSA energies achieve improved agreement with experiment. So at least in this system the accurate description of interaction energies that is provided by the DFT calculations is critical for the correct calculation of free energy differences.

As we have mentioned in the Introduction, force fields are significantly less computationally demanding than first principles quantum calculations, and this is reflected in our timings. For example, a single-point energy force field calculation on one of our complexes takes about 0.35 core seconds on an Intel CORE2 machine, while the same calculation with DFT takes about 24 core hours on the same computational platform. Therefore in terms of throughput, the force field calculations have a clear advantage. However, the point is that in several cases the unbiased and accurate description that is provided by the first principles calculations can be indispensanble. For example, electronic polarization, or halogen−π interactions, which are poorly described by available force fields. We therefore expect that large-scale first principles quantum calculations will be a valuable tool in the final stages of computational drug design where careful refinement is required. The linear-scaling formalism makes it feasible to extend the application of these calculations to biomolecules with thousands of atoms, especially in combination with new HPC technologies such as GPUs and peta-scale supercomputers.

4. CONCLUSIONS

In this paper we have presented an approach for reducing some of the limitations of the MM-PBSA method. Toward this aim we have used the ONETEP program to calculate the QM interaction energies with solvation contributions extracted from a traditional MM-PBSA method and scaled to match the QM energies. Conformational space was sampled with classical force field molecular dynamics simulations, and the compatibility of the structural ensemble, with respect to the potential energy surface, was checked by comparing forces on atoms between the two methods. These showed that, although there was substantial variation in the forces obtained with the two approaches, the forces in both cases were within expected ranges and that no unphysical conformations appear to be visited by the force field. This QM-PBSA approach obtained energies which are significantly improved over the MM computed energies, with enthalpic energies agreeing with experimental ΔH values to within 0.1 kcal mol^{-1}. The neglect of entropy leads to poor agreement with experimental absolute binding free energy values, however, relative binding free energies show considerable improvement agreeing well with experiment. These even show an improvement over the more rigorous TI method.

While the model we have studied is relatively simple and small (for biomolecular standards), it does include important and difficult to capture interactions, such as halogen−π interactions, which are not at all well described by force fields and even hydrogen bonds whose accurate description by nonquantum methods is reasonable but cannot be taken for granted. Therefore this is a small but important step toward modeling some of the crucial interactions in real protein−ligand systems. Armed with the experience from this study and with the ability of ONETEP for DFT calculations with thousands of atoms, we can in the future extend our investigation with QM-based free energy approaches to protein−ligand complexes of pharmaceutical interest. These typically include further challenges, such as rotatable bonds in the ligand, ligand and pocket desolvation, and partial solvation of the bound ligand in the case of solvent-exposed binding pockets.

AUTHOR INFORMATION

Corresponding Author
*E-mail: c.skylaris@soton.ac.uk.

ACKNOWLEDGMENT

S.F. would like to thank BBSRC for a CASE studentship award supported by Boehringer Ingelheim. C.-K.S. would like to thank the Royal Society for a University Research Fellowship. The calculations in this work were carried out on the Iridis3 Supercomputer of the University of Southampton. We would like to thank Dr. Danny Cole from the Theory of Condensed Matter group at the University of Cambridge for useful discussions.

REFERENCES

(1) Friesner, R. A.; Dunietz, B. D. *Acc. Chem. Res.* **2001**, *34*, 351–358.
(2) Halperin, I.; Ma, B. Y.; Wolfson, H.; Nussinov, R. *Proteins: Struct., Funct., Genet.* **2002**, *47*, 409–443.
(3) Kollman, P. A.; Massova, I.; Reyes, C.; Kuhn, B.; Huo, S.; Chong, L.; Lee, M.; Lee, T.; Duan, Y.; Wang, W.; Donini, O.; Cieplak, P.; Srinivasan, J.; Case, D. A.; Cheatham, T. E. *Acc. Chem. Res.* **2000**, *33*, 889–897.
(4) Still, W. C.; Tempczyk, A.; Hawley, R. C.; Hendrickson, T. *J. Am. Chem. Soc.* **1990**, *112*, 6127–6129.
(5) Michel, J.; Essex, J. *J. Comput.-Aided. Mol. Des.* **2010**, *24*, 639–658.
(6) Halgren, T. A.; Damm, W. *Curr. Opin. Struct. Biol.* **2001**, *11*, 236–242.
(7) Kohn, W.; Sham, L. J. *Phys. Rev.* **1965**, *140*, A1133–A1138.
(8) Kamerlin, S. C. L.; Haranczyk, M.; Warshel, A. *J. Phys. Chem. B* **2009**, *113*, 1253–1272.
(9) Riccardi, D.; Schaefer, P.; Yang, Y.; Yu, H. B.; Ghosh, N.; Prat-Resina, X.; Konig, P.; Li, G. H.; Xu, D. G.; Guo, H.; Elstner, M.; Cui, Q. *J. Phys. Chem. B* **2006**, *110*, 6458–6469.
(10) Goedecker, S. *Rev. Mod. Phys.* **1999**, *71*, 1085–1123.
(11) Skylaris, C.-K.; Haynes, P. D.; Mostofi, A. A.; Payne, M. C. *J. Chem. Phys.* **2005**, *122*, 084119.
(12) Bowler, D. R.; Bush, I. J.; Gillan, M. J. *J. Quant. Chem.* **2000**, *77*, 831–842.
(13) Soler, J. M.; Artacho, E.; Gale, J. D.; Garcia, A.; Junquera, J.; Ordejon, P.; Sanchez, D. *J. Phys.: Condens. Matter* **2002**, *14*, 2745–2779.
(14) Bowler, D. R.; Fattebert, J. L.; Gillan, M. J.; Haynes, P. D.; Skylaris, C.-K. *J. Phys.: Condens. Matter* **2008**, *20*, 290301.
(15) Fox, T.; Thomas, B. E., IV; McCarrick, M.; Kollman, P. A. *J. Phys. Chem.* **1996**, *100*, 10779–10783.
(16) Branda, N.; Wyler, R.; Rebek, J. *Science* **1994**, *263*, 1267–1268.
(17) Hine, N. D. M.; Haynes, P. D.; Mostofi, A. A.; Skylaris, C.-K.; Payne, M. C. *Comput. Phys. Commun.* **2009**, *180*, 1041–1053.
(18) Skylaris, C.-K.; Haynes, P. D.; Mostofi, A. A.; Payne, M. C. *Phys. Status Solidi* **2006**, *243*, 973–988.
(19) Skylaris, C.-K.; Mostofi, A. A.; Haynes, P. D.; Diéguez, O.; Payne, M. C. *Phys. Rev. B.* **2002**, *66*, 035119.
(20) Mostofi, A. A.; Haynes, P. D.; Skylaris, C.-K.; Payne, M. C. *J. Chem. Phys.* **2003**, *119*, 8842–8848.

(21) Haynes, P. D.; Skylaris, C.-K.; Mostofi, A. A.; Payne, M. C. *Chem. Phys. Lett.* **2006**, *422*, 345–349.
(22) Massova, I.; Kollman, P. A. *J. Am. Chem. Soc.* **1999**, *121*, 8133–8143.
(23) Diaz, N.; Suárez, D.; Merz, K. M.; Sordo, T. L. *J. Med. Chem.* **2005**, *48*, 780–791.
(24) Kaukonen, M.; Soderhjelm, P.; Heimdal, J.; Ryde, U. *J. Phys. Chem. B* **2008**, *112*, 12537–12548.
(25) Wang, M.; Wong, C. F. *J. Chem. Phys.* **2007**, *126*, 026101.
(26) Cole, D. J.; Skylaris, C.-K.; Rajendra, E.; Venkitaraman, A. R.; Payne, M. C. *Europhys. Lett.* **2010**, *91*, 37004.
(27) Hill, Q.; Skylaris, C.-K. *Proc. R. Soc. A* **2009**, *465*, 669–683.
(28) *MOE*, 2009.10; Chemical Computing Group, Inc.: Montreal, Canada, 2009.
(29) Case, D. A.; Darden, T.; Cheatham, T.; Simmerling, C.; Wang, J.; Duke, R.; Luo, R.; Crowley, M.; Roitberg, S. H. A.; Seabra, G.; Kolossváry, I.; Wong, K. F.; Paesani, F.; Vanicek, J.; Wu, X.; Brozell, S. R.; Steinbrecher, T.; Gohlke, H.; Yang, L.; Tan, C.; Mongan, J.; Hornak, V.; Cui, G.; Mathews, D.; Seetin, M.; C.,; Sagui,; Babin, V.; Kollman, P. A. *AMBER10*; University of California, San Francisco: San Francisco, CA, 2008.
(30) Wang, J.; Wolf, R. M.; Caldwell, J. W.; Kollman, P. A.; Case, D. A. *J. Comput. Chem.* **2004**, *25*, 1157–1174.
(31) Ryckaert, J.-P.; Ciccotti, G.; Berendsen, H. J. C. *J. Comput. Phys.* **1977**, *23*, 327–341.
(32) Perdew, J. P.; Burke, K.; Ernzerhof, M. *Phys. Rev. Lett.* **1996**, *77*, 3865–3868.
(33) Robinson, M.; Haynes, P. D. *J. Chem. Phys.* **2010**, *133*, 084109.
(34) Frisch, M. J.; Trucks, G. W.; Schlegel, H. B.; Scuseria, G. E.; Robb, M. A.; Cheeseman, J. R.; Scalmani, G.; Barone, V.; Mennucci, B.; Petersson, G. A.; Nakatsuji, H.; Caricato, M.; Li, X.; Hratchian, H. P.; Izmaylov, A. F.; Bloino, J.; Zheng, G.; Sonnenberg, J. L.; Hada, M.; Ehara, M.; Toyota, K.; Fukuda, R.; Hasegawa, J.; Ishida, M.; Nakajima, T.; Honda, Y.; Kitao, O.; Nakai, H.; Vreven, T.; Montgomery, J. J. A.; Peralta, J. E.; Ogliaro, F.; Bearpark, M.; Heyd, J. J.; Brothers, E.; Kudin, K. N.; Staroverov, V. N.; Kobayashi, R.; Normand, J.; Raghavachari, K.; Rendell, A.; Burant, J. C.; Iyengar, S. S.; Tomasi, J.; Cossi, M.; Rega, N.; Millam, J. M.; Klene, M.; Knox, J. E.; Cross, J. B.; Bakken, V.; Adamo, C.; Jaramillo, J.; Gomperts, R.; Stratmann, R. E.; Yazyev, O.; Austin, A. J.; Cammi, R.; Pomelli, C.; Ochterski, J. W.; Martin, R. L.; Morokuma, K.; Zakrzewski, V. G.; Voth, G. A.; Salvador, P.; Dannenberg, J. J.; Dapprich, S.; Daniels, A. D.; Farkas, Ö.; Foresman, J. B.; Ortiz, J. V.; Cioslowski, J.; Fox, D. J. *Gaussian 09*, revision A.1. Gaussian, Inc.: Wallingford, CT, 2009.
(35) Dunning, T. H. *J. Chem. Phys.* **1989**, *90*, 1007–1023.
(36) Becke, A. D. *J. Chem. Phys.* **1997**, *107*, 8554–8560.
(37) Grimme, S. *J. Comput. Chem.* **2006**, *27*, 1787–1799.
(38) Cornell, W. D.; Cieplak, P; Bayly, C. I.; Gould, I. R.; Merz, K. M.; Fergusson, D. M.; Spellmeyer, D. C.; Fox, T.; Caldwell, J. W.; Kollman, P. A. *J. Am. Chem. Soc.* **1995**, *117*, 5179–5197.